INSTITUTO SUPERIOR TÉCNICO

2ND CYCLE INTEGRATED PROJECT IN ENGINEERING PHYSICS

Linearized General Relativity in Hyperboloidal Coordinates

Author:
Filipe Ficalho

Supervisor:
Prof. David Hilditch

Research work performed for the Master in Engineering Physics

at

January 11, 2025

1 Introduction

When studying gravitational waves, we must be mindful that gravitational wave sources (like black hole mergers, neutron stars, etc.) are billions of light years away from Earth. From the point of view of an observer on Earth, this distance is so vast that it can be approximated as being at infinity. This distance, however, is not sufficiently far away to require accounting for the cosmological constant, allowing us to model spacetime as asymptotically flat. Thus, we are interested in studying the behavior of the gravitational fields at null infinity, $\mathscr{I}$.

To do so, we may perform a conformal compactification of the spacetime, which brings $\mathscr{I}$ to a finite distance on our computational grid. This is done by working in the hyperboloidal coordinate system.

1.1 Hyperboloidal Coordinates

The hyperboloidal coordinate system, as previously mentioned, maps our previously unbonded domain to a finite one by introducing new time and radial coordinates (t, r), which are related to the spherical coordinates of Minkowski spacetime (T, R) by the transformations

$$t = T - H(R) \qquad\qquad R = \frac{r}{\Omega(r)} \,, \tag{1}$$

where $H(R)$ is called the height function and $\Omega(r)$ is called the compress function [1, 2], which give rize to the Jacobian matrix:

$$\left(J^{Hyp}\right)_{\alpha'}^{\ \beta} = \begin{pmatrix} 1 & -H'(r) & 0 & 0 \\ 0 & \frac{L(r)}{\Omega^2(r)} & 0 & 0 \\ 0 & 0 & 1 & 0 \\ 0 & 0 & 0 & 1 \end{pmatrix} \,, \tag{2}$$

where $H'(r)$ denotes the derivative of the height function with respect to R written as a function of r, and $L(r)$ is defined as

$$L(r) \equiv \Omega(r) - r\,\partial_r\Omega(r) \,. \tag{3}$$

This coordinate system is advantageous because it allows us to do the desired compactification while maintaining the characteristic speed of outgoing waves finite. Additionally, we can choose the height and compress functions so that the outgoing light speed is constant, which we can observe in figure 1 for a specific choice of the height and compress functions [1]. In contrast, this coordinate system makes incoming waves hard to resolve.

Throughout this work, we will sacrifice this very relevant property in exchange for ease of manipulation of the expressions since the goal of this introductory work to the subject is to get accustomed to the coordinate system. The height and compress functions that will used throughout this work are

$$H(R) = \sqrt{S^2 + R^2} \qquad\qquad \Omega(r) = \tfrac{1}{2}\left(1 - \tfrac{r^2}{S^2}\right) \,, \tag{4}$$

where S is a constant that determines the size of the compactified domain, which we can choose arbitrarily. To make our domains range from -1 to 1 in the generic case and from 0 to 1 in the spherically symmetric case, we will set $S = 1$. As a consequence of our previous choices, we also have

$$H'(r) = \tfrac{2\,r\,S}{S^2+r^2} \qquad\qquad L(r) = \tfrac{1}{2}\left(1 + \tfrac{r^2}{S^2}\right) \,. \tag{5}$$

For this choice of functions, we still have that the incoming light speed decreases as it reaches $\mathscr{I}$. However, we don't have a constant outgoing propagation speed, shown in figure 2. The only implication this choice will have in our results is that the wave will take longer to reach $\mathscr{I}$ and will be

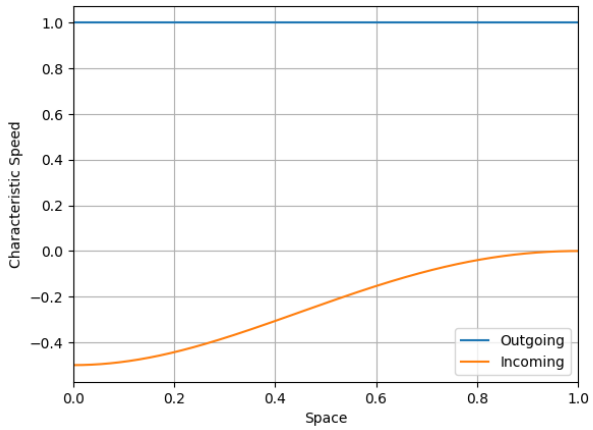

FIGURE 1: Characteristic speeds of the wave equation in hyperboloidal coordinates with $H(R) = \frac{2R^2+S^2-\sqrt{4R^2S^2+S^4}}{2R}$, $\Omega(r) = 1 - \frac{r^2}{S^2}$ and $S = 1$ for outgoing and incoming waves.

slightly distorted, which is not problematic since our purpose is to ensure the code converges smoothly toward the solution.

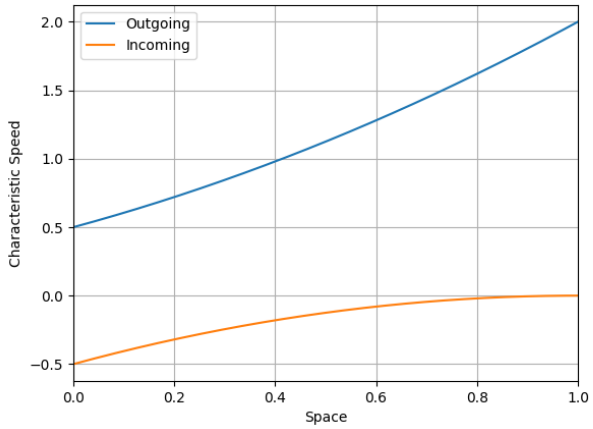

FIGURE 2: Characteristic speeds of the wave equation in hyperboloidal coordinates with $H(R) = \sqrt{S^2 + R^2}$, $\Omega(r) = \frac{1}{2}\left(1 - \frac{r^2}{S^2}\right)$ and $S = 1$ for outgoing and incoming waves.

1.2 Computational Setup

This work is a continuation of my previous work on numerical relativity. As such, the framework used here is the same as the one used there (described in [3]), with the addition of truncation error matching for the derivatives, interpolation at the boundaries, and the Evans Method for regularization at the origin.

1.2.1 Truncation Error Matching

Truncation error matching is a technique used to improve the accuracy of the numerical solution by matching the truncation error of the finite difference scheme used on the boundaries to the truncation error of the one used in the interior of our computational domain. This matching uses a one-sided

finite difference scheme on the boundaries such that the leading order error term is the same as the one used in the interior.

In our framework, to approximate the first derivative of a field ψ at an interior point i (writing the leading order error term explicitly), we use

$$\psi'_i = \frac{\psi_{i+1} - \psi_{i-1}}{2h} - \frac{h^2}{6}\psi'''_i + \dots , \tag{6}$$

where ψ_{i+1} and ψ_{i-1} are the values of the field ψ at the points $i+1$ and $i-1$ respectively, and h is the grid spacing. [4, 5]

To match this leading order term of the error at the left and right boundary points, respectively, we use

$$\psi'_i = \frac{\psi_{i+3} - 4\psi_{i+2} + 7\psi_{i+1} - 4\psi_i}{2h} - \frac{h^2}{6}\psi'''_i + \dots \tag{7}$$

$$\psi'_i = \frac{4\psi_i - 7\psi_{i-1} + 4\psi_{i-2} - \psi_{i-3}}{2h} - \frac{h^2}{6}\psi'''_i + \dots \tag{8}$$

1.2.2 Extrapolation at the Boundaries

Since we are interested in evolving the fields at null infinity, we must choose a boundary condition that allows the fields to propagate out of our computational domain. To do so, we use extrapolation at the outer boundaries of our computational domain to fill the ghost points in those regions. We calculate the value of our fields at the ghost points using

$$\psi_i = 4\psi_{i-1} - 6\psi_{i-2} + 4\psi_{i-3} - \psi_{i-4} , \tag{9}$$

where ψ_i is the value of the field at the ghost point i, and ψ_{i-1}, ψ_{i-2}, ψ_{i-3} and ψ_{i-4} are the values of the field at the points $i-1$, $i-2$, $i-3$ and $i-4$ respectively.

1.2.3 Evans Method

When dealing with operators like the Laplacian in spherical coordinates, we find some formal singularities, like terms where the coefficients are inversely proportional to the radial coordinate, that we must remove for our code to work. To remove those singularities, we can apply the Evans Method. This method involves rewriting the singular terms as a different differential operator, called the Evans operator, which we can evaluate at the grid points. We define this operator as

$$\partial_r\psi + \frac{p}{r}\psi = (p+1)\frac{d(r^p\psi)}{dr^{p+1}} , \tag{10}$$

where p is a constant. This operator can be expressed in terms of the grid points as

$$(p+1)\frac{d(r^p\psi)}{dr^{p+1}} = (\tilde{D}\psi)_i = (p+1)\frac{r^p_{i+1}\psi_{i+1} - r^p_{i-1}\psi_{i-1}}{r^{p+1}_{i+1} - r^{p+1}_{i-1}} , \tag{11}$$

where the subscripts $i+1$ and $i-1$ denote the grid points $i+1$ and $i-1$ respectively. [6]

2 Wave Equation in 1+1 Dimensions

Let us start by considering the wave equation in 1+1 dimensions:

$$\Box\psi \equiv -\partial_T^2\psi + \partial_X^2\psi = 0 . \tag{12}$$

From my previous work on the subject [], we concluded that we should use systems of equations that are first order both in space and time since the second order in space and first order in time scheme created problems for us in that same work. Thus, we should perform a first-order reduction of the wave equation before proceeding. Defining $\Pi \equiv -\partial_T \psi$, we obtain

$$\begin{cases} \partial_T \psi = -\Pi \\ \partial_T \Pi = -\partial_{\underline{i}} \partial^{\underline{i}} \psi \end{cases} , \tag{13}$$

to which we can add the constraint $C_{\underline{i}} = \partial_{\underline{i}} \psi - \Phi_{\underline{i}} \overset{!}{=} 0$ to our system of equations, to which small violations could be allowed. Using the time derivative of this constraint as an evolution equation for Φ and expressing the violation of this constraint as $\gamma_2 C_{\underline{i}}$, where γ_2 is a parameter corresponding to the allowed violation, we get

$$\begin{cases} \partial_T \psi = -\Pi \\ \partial_T \Phi = -\partial_X \Pi + \gamma_2 \, \partial_X \psi - \gamma_2 \, \Phi \\ \partial_T \Pi = -\partial_X \Phi \end{cases} . \tag{14}$$

We then proceed with a coordinate change from inertial Minkowski coordinates to hyperboloidal coordinates. Additionally, even though we could allow for slight violations of our constraint, we will not. Thus, we set $\gamma_2 = 0$, obtaining the final form of our system of equations:

$$\begin{cases} \partial_t \psi = -\Pi \\ \partial_t \Phi = \mathcal{A} \, \left(H' \, \partial_x \Phi + \partial_x \Pi \right) \\ \partial_t \Pi = \mathcal{A} \, \left(H' \, \partial_x \Pi + \partial_x \Phi \right) \end{cases} , \tag{15}$$

where we defined $\mathcal{A}(x) = \frac{\Omega^2(x)}{L(x)(H'^2(x)-1)}$, and dropped the explicit dependences on x to simplify the notation.

We can now solve this system of equations by applying truncation error matching for the derivatives on the boundaries and turning off the artificial dissipation on those points. Using that framework and giving the initial conditions

$$\psi(0,x) = A \, e^{-C \, x^2/2} \, , \quad \Phi(0,x) = -A \, C \, x \, \frac{\Omega^2(x)}{L(x)} \, e^{-C \, x^2/2} \quad \text{and} \quad \Pi(0,x) = 0 \, , \tag{16}$$

with $A = 1$ and $C = 100$, we obtain the evolution present in figure 3. In that evolution, it is noticeable that after the wave propagates out of the computational domain, there is a negative displacement that does not disperse as one would naively think would happen. Even though this result is counterintuitive, it was proven correct in [7].

Doing a norm convergence test (using the L^2 norm), we obtain a clean second-order convergence during the whole evolution, as can be seen for ψ in the left of figure 4. We can also see that these results stay promising up until $\mathscr{I}$ through the pointwise convergence at that point, represented in the right of figure 4.

3 Wave Equation in 3+1 Dimensions With Spherical Symmetry

Now, let us consider the wave equation in 3+1 dimensions with spherical symmetry:

$$\Box \psi \equiv -\partial_T^2 \psi + \frac{1}{R^2} \partial_R \left(R^2 \partial_R \psi \right) = 0 \, . \tag{17}$$

Since ψ is a solution to this equation, it will decay at a rate of $1/R$, which is a problem because we want to know how our field behaves at $\mathscr{I}$. Thus, we need to renormalize this field so it does not vanish at

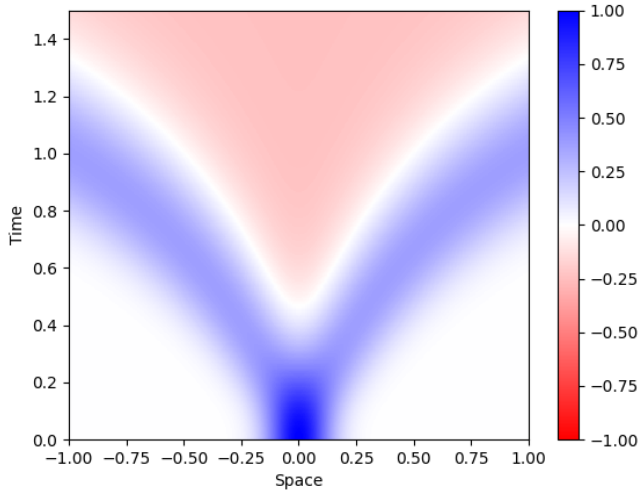

FIGURE 3: Evolution of the wave equation in 1+1 dimensions using hyperboloidal coordinates with the initial conditions given in equation (16), with $A = 1$ and $C = 100$.

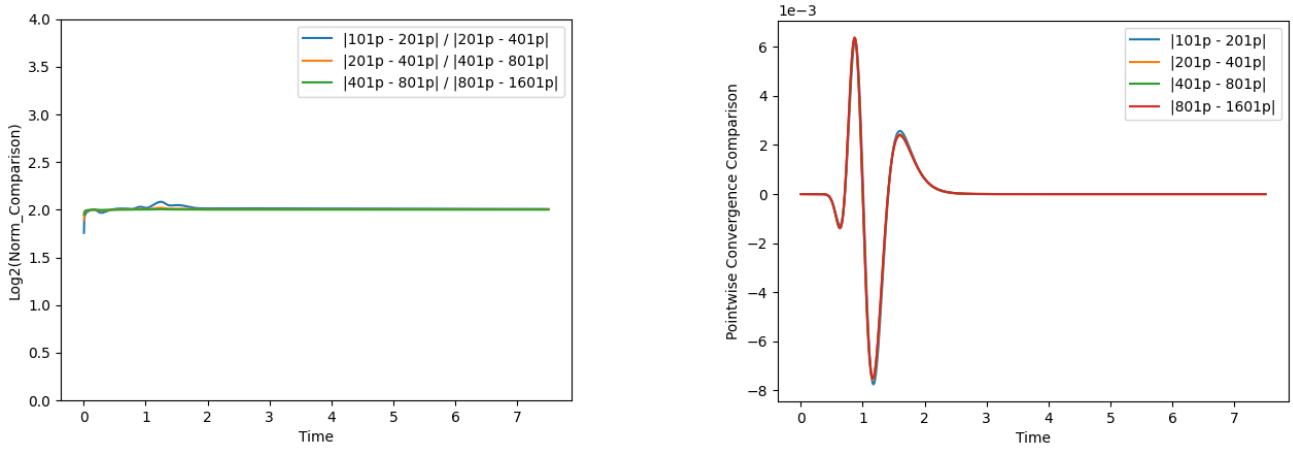

FIGURE 4: Convergence tests for the evolution of the wave equation in 1+1 dimensions using hyperboloidal coordinates, provided the initial conditions given in equation 16, with $A = 1$ and $C = 100$. On the left, we have the L^2 norm convergence, and on the right, we have the pointwise convergence at $\mathscr{I}$.

infinity. With this in mind, let us define a new field Ψ such that

$$\Psi \equiv \chi\,\psi\,, \tag{18}$$

where we will take $\chi = \sqrt{1+R^2}$.

Applying that transformation to the equation, it becomes

$$\partial_T^2\Psi = \partial_R^2\Psi + \frac{2}{R(R^2+1)}\partial_R\Psi - \frac{3}{(R^2+1)^2}\Psi\,, \tag{19}$$

to which we can apply a first-order reduction, obtaining

$$\begin{cases} \partial_T\Psi = -\Pi \\ \partial_T\Phi = -\partial_R\Pi + \gamma_2\partial_R\Psi - \gamma_2\Phi \\ \partial_T\Pi = -\partial_R\Phi - \frac{2}{R(R^2+1)}\Phi + \frac{3}{(R^2+1)^2}\Psi \end{cases}. \tag{20}$$

Doing a coordinate change from inertial Minkowski coordinates to hyperboloidal coordinates and setting $\gamma_2 = 0$ as we did previously, we get

$$\begin{cases} \partial_T \Psi = -\Pi \\ \partial_T \Phi = \mathcal{B}\left((r^2+\Omega^2)^2\left(H'\partial_r\Phi + \partial_r\Pi\right) + H'L\Omega\left(2r\Phi - 3\Omega\Psi + 2r^{-1}\Omega^2\Phi\right)\right) \\ \partial_T \Pi = \mathcal{B}\left((r^2+\Omega^2)^2\left(\partial_r\Phi + H'\partial_r\Pi\right) + L\Omega\left(2r\Phi - 3\Omega\Psi + 2r^{-1}\Omega^2\Phi\right)\right) \end{cases}, \tag{21}$$

where we defined $\mathcal{B} = \frac{\Omega^2}{L(H'^2-1)(r^2+\Omega^2)^2}$.

We can see that in our evolution equations for Φ and Π, there are formally singular terms we can remove by applying the Evans method. For that, we rewrite those evolution equations, obtaining

$$\begin{cases} \partial_T \Psi = -\Pi \\ \partial_T \Phi = \mathcal{B}\left((r^2+\Omega^2)^2\left(H'\partial_r\Phi + \partial_r\Pi\right) + H'L\Omega\left(2r\Phi - 3\Omega\Psi - \Omega^2\partial_r\Phi\right) + H'L\Omega^3\left(\partial_r\Phi + 2r^{-1}\Phi\right)\right) \\ \partial_T \Pi = \mathcal{B}\left((r^2+\Omega^2)^2\left(\partial_r\Phi + H'\partial_r\Pi\right) + L\Omega\left(2r\Phi - 3\Omega\Psi - \Omega^2\partial_r\Phi\right) + L\Omega^3\left(\partial_r\Phi + 2r^{-1}\Phi\right)\right) \end{cases}, \tag{22}$$

where we can directly apply the Evans method to the last terms in parenthesis.

Imposing the parity of each field at the origin and doing extrapolation at $\mathscr{I}$ (instead of truncation error matching that we used before) as our boundary conditions and using the initial data

$$\psi(0,r) = A\, e^{-C\, r^2/2}\,, \quad \Phi(0,r) = -A\, C\, r\, \frac{\Omega^2(r)}{L(r)}\, e^{-C\, r^2/2} \quad \text{and} \quad \Pi(0,r) = 0\,, \tag{23}$$

with $A = 1$ and $C = 100$, we obtain the evolution represented in figure 5.

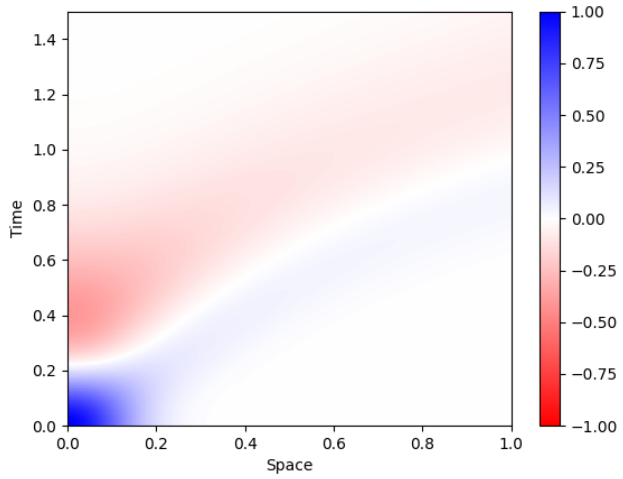

FIGURE 5: Evolution of the wave equation in 3+1 dimensions with spherical symmetry using hyperboloidal coordinates with the initial conditions given in equation (23), with $A = 1$ and $C = 100$.

Similarly to the previous case, we obtain a clean second-order convergence during the whole evolution, shown in the left of figure 6 for ψ, and an excellent pointwise convergence at $\mathscr{I}$, as seen in the right of figure 6. Even though these results are already outstanding, they could be further improved by using truncation error matching at the outer boundary instead of extrapolation.

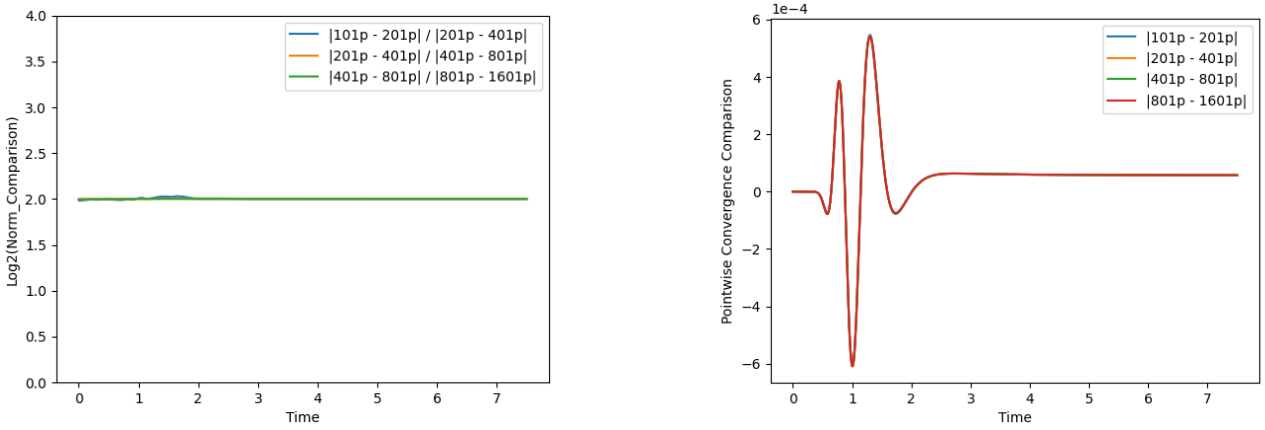

FIGURE 6: Convergence tests for the evolution of the wave equation in 3+1 dimensions with spherical symmetry using hyperboloidal coordinates, provided the initial conditions given in equation (23), with $A = 1$ and $C = 100$.. On the left, we have the L^2 norm convergence, and on the right, we have the pointwise convergence at $\mathscr{I}$.

4 Cubic Wave Equation in 3+1 Dimensions With Spherical Symmetry

It is finally time to tackle non-linear variations of the wave equation in 3+1 dimensions with spherical symmetry. We start by writing the wave equation as

$$\Box\psi \equiv -\partial_T^2\psi + \frac{1}{R^2}\partial_R\left(R^2\partial_R\psi\right) = \psi^3 \,. \tag{24}$$

By applying a first-order reduction followed by the coordinate change to hyperboloidal coordinates and setting $\gamma_2 = 0$, we get

$$\begin{cases} \partial_T\Psi = -\Pi \\ \partial_T\Phi = \mathcal{B}\left((r^2+\Omega^2)^2\left(H'\partial_r\Phi + \partial_r\Pi\right) + H'L\Omega\left(2r\Phi - 3\Omega\Psi + 2r^{-1}\Omega^2\Phi\right)\right) + \frac{\mathcal{A}LH'}{r^2+\Omega^2}\Psi^3 \\ \partial_T\Pi = \mathcal{B}\left((r^2+\Omega^2)^2\left(\partial_r\Phi + H'\partial_r\Pi\right) + L\Omega\left(2r\Phi - 3\Omega\Psi + 2r^{-1}\Omega^2\Phi\right)\right) + \frac{\mathcal{A}L}{r^2+\Omega^2}\Psi^3 \end{cases} , \tag{25}$$

where we used the previous definitions for $\mathcal{A}$ and $\mathcal{B}$.

Differently from the linear case, where we expect Gaussian initial conditions that only differ by amplitude to behave similarly, we reckon that parameter highly influences the solution. We will investigate this by solving the cubic wave equation with different initial conditions and comparing the results. Using the same boundary conditions as we did previously and using the initial conditions

$$\psi(0,r) = A\,e^{-C\,r^2/2}\,, \quad \Phi(0,r) = -A\,C\,r\,\frac{\Omega^2(r)}{L(r)}\,e^{-C\,r^2/2} \quad \text{and} \quad \Pi(0,r) = 0 \,, \tag{26}$$

with $A = 1.0$ for one of the runs and $A = 10.0$ for the other, while keeping $C = 10$ we get the results shown in figure 7. We can see that, for $A = 1$, we get a solution that behaves very similarly to the linear one, as the wave starts to disperse. However, compared to the linear solution, it takes longer to disperse as there is a source term. For $A = 10$, we get a solution that grows rapidly until it explodes.

Despite behaving differently in both cases, our solutions show similar convergence. For $A = 1$, our solution converges cleanly in the norm and pointwise convergence tests, as shown in figure 8, which is to be expected due to the similarity to the linear solution and our previous results. For $A = 10$, we obtain the same second-order convergence until the analytical blowup, as shown in figure 9.

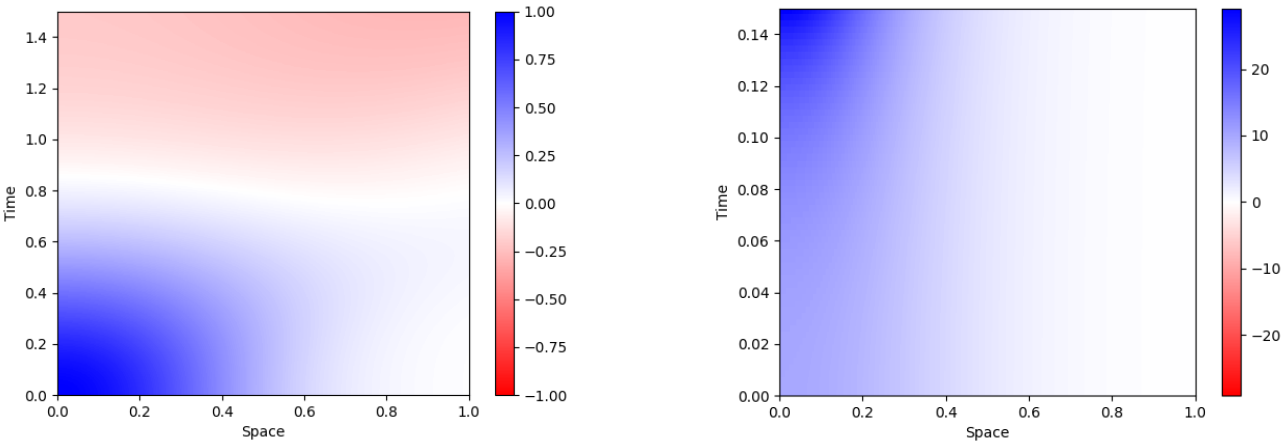

FIGURE 7: Evolution of the cubic wave equation in 3+1 dimensions with spherical symmetry using hyperboloidal coordinates with the initial conditions given in equation (26). On the left, we have $A = 1$ and $C = 10$. On the right, we have $A = 10$ and $C = 10$.

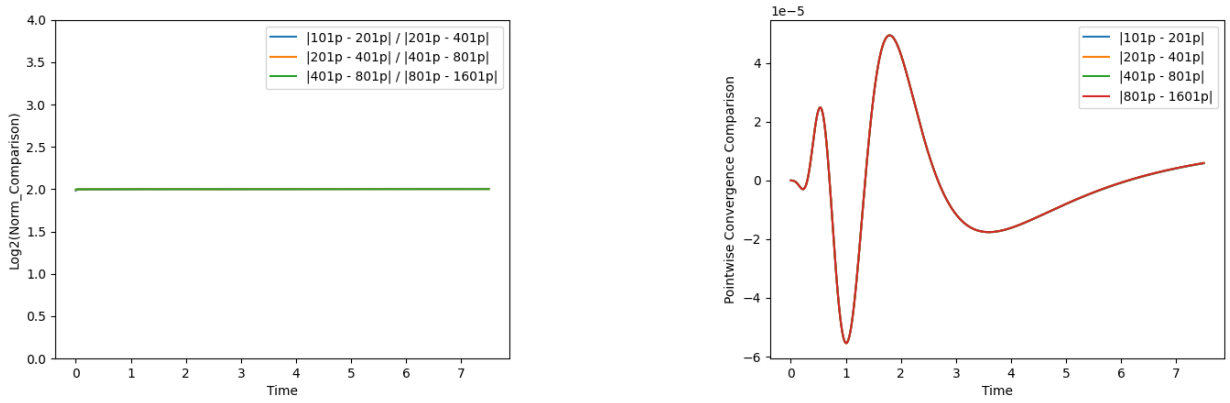

FIGURE 8: Convergence tests of the evolution of the cubic wave equation in 3+1 dimensions with spherical symmetry using hyperboloidal coordinates, provided the initial conditions given in equation (26), with $A = 1$ and $C = 10$. On the left, we have the L^2 norm convergence, and on the right, we have the pointwise convergence at $\mathscr{I}$.

5 Incoming Waves in Hyperboloidal Coordinates

As seen previously, when using hyperboloidal coordinates, we expect incoming waves to be hard to resolve, as the error associated with them is expected to grow very rapidly as the wave propagates. We will quantify that error by using incoming waves as initial conditions and comparing the numerical solution with the exact one. It is then possible to study how much the error grows with the distance traveled toward the origin by doing several runs with the starting pulse further and further away.

First, we must build initial conditions that are purely incoming. We do that by doing a linear combination of an incoming and an outgoing wave while making sure that the solution decays with $1/R$, that is

$$\psi(T, R) = \frac{f(T + R) - f(T - R)}{R}, \tag{27}$$

where we have the liberty to choose the function f. To obtain a purely incoming wave, we can choose f so the outgoing wave vanishes in our computational domain. We will take f to be a Gaussian pulse

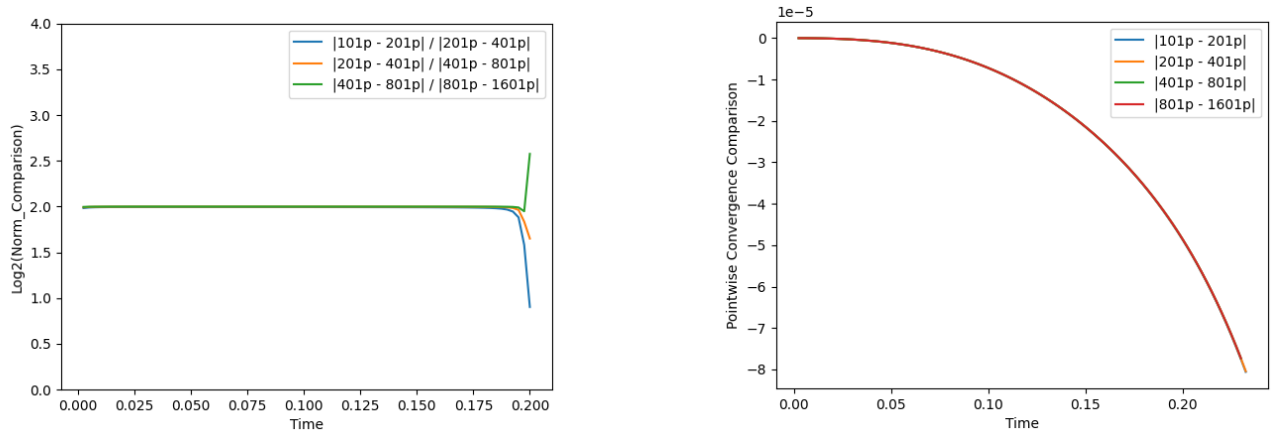

FIGURE 9: Convergence tests of the evolution of the cubic wave equation in 3+1 dimensions with spherical symmetry using hyperboloidal coordinates, provided the initial conditions given in equation (26), with $A = 10$ and $C = 10$. On the left, we have the L^2 norm convergence, and on the right, we have the pointwise convergence at $\mathscr{I}$.

given by

$$f(x) = e^{-C(x-x_0)^2/2}, \tag{28}$$

where x_0 shifts the center of the pulse and C determines the width of the pulse, and we will consider $C = 100$. Thus, the complete set of initial conditions is

$$\psi(T,R) = \frac{f(T+R)-f(T-R)}{R} \quad \Phi(T,R) = -\frac{f'(T+R)-f'(T-R)}{R} \quad \Pi(T,R) = \frac{(f'(T+R)-f'(T-R))R-(f(T+R)-f(T-R))}{R^2} \tag{29}$$

where f' is the derivative of f. We now apply the change to hyperboloidal coordinates (where we defined a slightly modified height function $H(R) = \sqrt{S^2+R^2} - S$ to make t and T coincide at $R = 0$) and run several simulations for the wave equation in 3+1 dimensions with spherical symmetry (without applying the rescaling of the fields) up until the center of the pulse reaches the origin while ranging x_0 from 1 to 10. The initial conditions for each pulse and the variation in time of the norm of the exact error normalized to the norm of the solution can be found in figure 10.

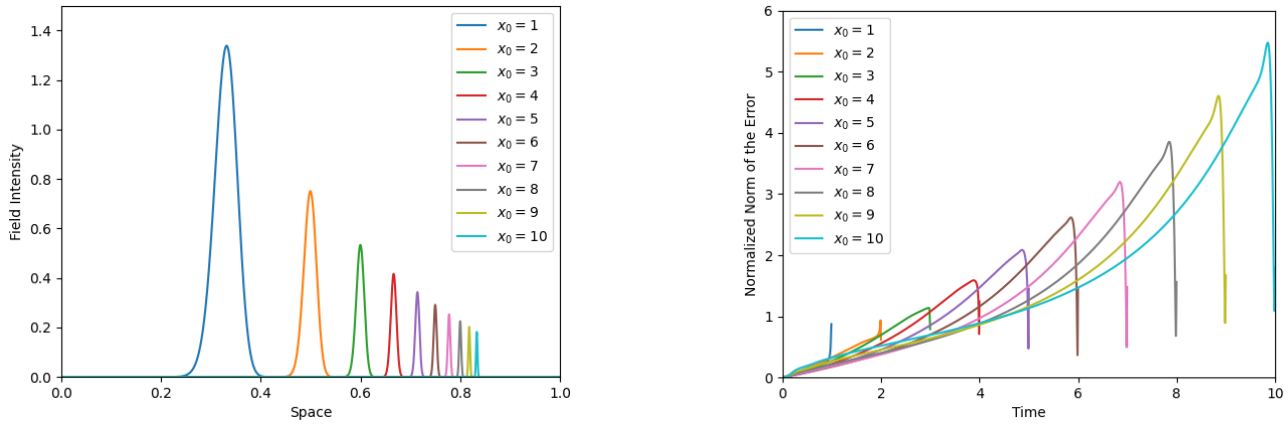

FIGURE 10: Initial conditions for ψ (left) and the variation in time of the norm of the exact error normalized to the norm of the solution (right).

We can see just by the initial conditions that incoming waves become more difficult to resolve the further away they are, as the Gaussian gets thinner the closer it is to $\mathscr{I}$. Additionally, we can see that the error increases very rapidly as the waves propagate. Both these results were what we would

expect to happen for this coordinate system. Therefore, if we expect incoming waves on our system, we should modify the coordinates to have a traditional Cauchy slice for part of the domain and then join that slice to a hyperboloidal slice when we don't expect to have incoming waves anymore.

6 Conclusions

Throughout this work, the hyperboloidal coordinate system proved to be a very advantageous and convenient tool when studying the behavior of outgoing waves. Our numerical experiments demonstrated the reliability of our code framework when dealing with different variations of the wave equation in these coordinates by showing clean second-order convergence in all the performed simulations.

However, this choice of coordinates is not adequate when there are incoming waves in our problem since they are very hard to resolve and are great sources of error in the simulations. This suggests that a hybrid approach may be ideal for the cases where we expect to have incoming waves in a small portion of our domain, incorporating traditional Cauchy slices alongside hyperboloidal ones.

The master thesis that follows this project will focus on expanding the well-established numerical relativity code `BAMPS`, making it able to perform simulations in this coordinate system. In addition, we will look into more intricate nonlinearities with both mathematical and physical significance such as the wave equation with quadratic nonlinearity, as we try to get closer to solving the Einstein equations numerically.

References

[1] David Hilditch et al. *The evolution of hyperboloidal data with the dual foliation formalism: Mathematical analysis and wave equation tests*. 2016. arXiv: 1609.08949 [gr-qc]. URL: https://arxiv.org/abs/1609.08949.

[2] Anıl Zenginoğlu. "Hyperboloidal layers for hyperbolic equations on unbounded domains". In: *Journal of Computational Physics* 230.6 (Mar. 2011), 2286–2302. ISSN: 0021-9991. DOI: 10.1016/j.jcp.2010.12.016. URL: http://dx.doi.org/10.1016/j.jcp.2010.12.016.

[3] Filipe Ficalho. "Numerical Evolutions of Spacetime". Available at https://ulisboa-my.sharepoint.com/:b:/g/personal/ist199933_tecnico_ulisboa_pt/EWrk5DmaLeRLmczdoGGSitYB46y_dfQVd4tsFxDF29MwmA?e=1r0FVY. 1st Cycle Integrated Project in Engineering Physics. Lisbon, Portugal: Instituto Superior Técnico, June 2023.

[4] Franz Pretorius. "Numerical Simulations of Gravitational Collapse". Available at http://laplace.physics.ubc.ca/Members/matt/Doc/Theses/Phd/pretorius.pdf. PhD thesis. Vancouver, Canada: University of British Columbia, Aug. 2002.

[5] Shalabh Gautam et al. "Summation by parts and truncation error matching on hyperboloidal slices". In: *Physical Review D* 103.8 (Apr. 2021). ISSN: 2470-0029. DOI: 10.1103/physrevd.103.084045. URL: http://dx.doi.org/10.1103/PhysRevD.103.084045.

[6] Charles Ross Evans. "Simulation of Axisymmetric Gravitational Collapse". Available at https://users.physics.unc.edu/~evans/cr_evans_thesis_1984.pdf. PhD thesis. Austin, USA: University of Texas, Aug. 1984.

[7] Juan A. Valiente Kroon and Lidia J. Gomes Da Silva. "The d'Alembert solution in hyperboloidal foliations". In: *General Relativity and Gravitation* 56.7 (July 2024). ISSN: 1572-9532. DOI: 10.1007/s10714-024-03272-2. URL: http://dx.doi.org/10.1007/s10714-024-03272-2.